Texture Analysis and Classification of ERS SAR Images for Map Updating of Urban Areas in The Netherlands

Rob J. Dekker

***Abstract*—In single-band and single-polarized synthetic aperture radar (SAR) image classification, texture holds useful information. In a study to assess the map-updating capabilities of such sensors in urban areas, some modern texture measures were investigated. Among them were histogram measures, wavelet energy, fractal dimension, lacunarity, and semivariograms. The latter were chosen as an alternative for the well-known gray-level cooccurrence family of features. The area that was studied using a European Remote Sensing Satellite 1 (ERS-1) SAR image was the conurbation around Rotterdam and The Hague in The Netherlands. The area can be characterized as a well-planned dispersed urban area with residential areas, industry, greenhouses, pasture, arable land, and some forest. The digital map to be updated was a 1 : 250 000 Vector Map (VMap1). The study was done on the basis of nonparametric separability measures and classification techniques because most texture distributions were not normal. The conclusion is that texture improves the classification accuracy. The measures that performed best were mean intensity (actually no texture), variance, weighted-rank fill ratio, and semivariogram, but the accuracies vary for different classes. Despite the improvement, the overall classification accuracy indicates that the land-cover information content of ERS-1 leaves something to be desired.**

***Index Terms*—Image classification, image texture analysis, synthetic aperture radar (SAR), terrain mapping, urban areas.**

I. Introduction

AUTOMATIC or semiautomatic map updating using remote sensing images is an important area of research. A growing amount of remote sensing information is available today from different types of sensors. A certain level of automation can speed-up the map updating process considerably. Synthetic aperture radar (SAR) sensors are interesting when information needs to be available urgently because they are independent of the weather condition and time of day (or night).

To study the capability of satellite SAR sensors for map updating, a European Remote Sensing Satellite 1 (ERS-1) image was used. Sensors such as the ERS-1/2, Envisat, and Radarsat-1 deliver images with a resolution of about 25 m, which is appropriate to update 1 : 250 000 maps (100 image pixels per map centimeter). Most are single band and single polarized, which limits the information to intensity and texture. Only Envisat is dual polarized. In tandem configuration, i.e., one-day repeat pass, the coherence can be used for map updating [7], [23].

Future SAR satellites will be dual or fully polarized (e.g., Radarsat-2, Cosmo/SkyMed, and TerraSAR) and can supply polarimetric information for map updating using polarimetric decomposition techniques [6], [10], [13]. Besides, they will have a better resolution (<5 m), which will result in different textures [28]. Unfortunately, this type of information is not available from ERS-1.

In map updating using ERS-1, one of the most interesting questions is which texture measures can best be used for discriminating different types of (urban) land cover, in addition to the image intensity. In an attempt to find the answer, data of the Randstad Holland (The Netherlands), including Rotterdam and The Hague was used. The area can be characterized as a well-planned dispersed urban area with residential areas, industry, greenhouses, pasture, arable land, and some forest. Previous results were presented in [32] and [33].

In this paper, an overview of modern texture measures is given (Section II). The same section presents methods for separability analysis and classification. In Section III, the results of the texture measures, separability analysis and classification are discussed. Conclusions are drawn in Section IV.

II. Texture, Analysis, and Classification

A. Texture Measures

If SAR sensors are single band and single polarized, besides intensity, texture is the only information available to study land cover for map updating. A great number of texture measures have been developed through the years. Based on an extensive study of literature, a set of promising measures was selected. Following below is a description of these measures.

1) Histogram Measures: The most common class of texture measures is the class of histogram measures. Well known are the mean (μ), mean Euclidean distance, variance (σ^2), skew, kurtosis, entropy (H), and energy (E) [11], [27]

$$\mu = \frac{\sum_{i,j} x_{ij}}{n} \tag{1}$$

$$\text{mean Euclidean distance} = \frac{\sqrt{\sum_{i,j}(x_{ij} - x_c)^2}}{n-1} \tag{2}$$

$$\sigma^2 = \frac{\sum_{i,j}(x_{ij} - \mu)^2}{n-1} \tag{3}$$

$$\text{skew} = \frac{\sum_{i,j}(x_{ij} - \mu)^3}{(n-1)\sigma^3} \tag{4}$$

$$\text{kurtosis} = \frac{\sum_{i,j}(x_{ij} - \mu)^4}{(n-1)\sigma^4} \tag{5}$$

Manuscript received September 11, 2002; revised March 12, 2003.

The author is with the TNO Physics and Electronics Laboratory (TNO-FEL), 2509 JG The Hague, The Netherlands (e-mail: r.j.dekker@fel.tno.nl).

Digital Object Identifier 10.1109/TGRS.2003.814628

$$H = -\sum_{i,j} p_{ij} \log(p_{ij}) \text{ with } p_{ij} = \frac{x_{ij}}{\sum_{i,j} x_{ij}} \tag{6}$$

$$E = \sum_{i,j} x_{ij}^2. \tag{7}$$

Here x_{ij} stands for the pixel value of pixel (i, j) in the kernel over which is summed, n for the number of pixels that is summed, x_c for the kernel's center pixel value, and p_{ij} for the normalized pixel value. Another histogram texture measure is the weighted-rank fill ratio, which is defined by Novak *et al.* [19]

$$\eta = \frac{\text{sum } \kappa\% \text{ brightest pixels}}{\text{sum all pixels}}. \tag{8}$$

A common value for κ is 5%.

2) Wavelet Energy Measures: The wavelet transform is a multiresolution decomposition. It can be interpreted as the inverse Fourier transforms of the set of logarithmically divided frequency bins [5]. Each decomposition level consists of four components: a highpass, a lowpass, a horizontal, and a vertical component. Starting at the highest level, every lowpass component can be decomposed into four new components until the lowest frequency is reached. Of all components only the high- and lowpass components are invariant. The other two components show a preference for structures in horizontal or vertical directions. Entropy and energy (6) and (7) of the different components are a measure of texture. The energy was used because it gave better classification results [16]. Bellagente *et al.* [2] compared different wavelet transforms for texture characterization, and concluded that the Daubechies wavelet with four coefficients (DAUB4) resulted in the highest classification accuracy.

3) Fractal Dimension: Fractal-based descriptions have been used successfully in texture analysis and segmentation of images [21]. Descriptors can be derived from the definition of the mass of a fractal surface within a window [15], [21]

$$M(r) = \Lambda r^{-K}. \tag{9}$$

Here M stands for the mass, r for the size (i.e., area) of the window, Λ for the lacunarity and K for the Hurst or persistence parameter. The lacunarity is, as is the mass, a function of the observation scale or window size r. The persistence parameter is related to the fractal dimension D by

$$K = 3 - D. \tag{10}$$

Originally this relation is written as $K = D_E - D$, in which D_E stands for the Euclidean dimension. $D_E = D_T + 1$, in which D_T is the topological dimension. For a surface function $D_T = 2$ and subsequently $D_E = 3$ [24].

Several methods exist to estimate the fractal dimension [1], [19], [21], [24]. Stewart *et al.* [24] concluded that the power spectral-density method is the most accurate. In this method, the fractal dimension can be derived from the slope of the log–log power spectrum of an image of the relation

$$\langle P(f) \rangle \propto f^{-\beta} \quad \beta = 2K + 2. \tag{11}$$

Here $P(f)$ stands for the log–log power spectrum in a certain direction, and f for the frequency. Based on this method, Alparone *et al.* [1] developed an alternative method using the wavelet transform. They found that this slope can also be obtained by a linear regression of the log energy of the wavelet components, versus the log of the frequency of each component, which is a power of two. In other words, a linear regression of all (x_j, y_j) for which

$$x_j = j \quad y_j = \frac{\log E_j}{\log 2}. \tag{12}$$

Here E_j stands for the total energy of the invariant wavelet component of level j using (7). Equation (12) is different from that in [1], [32], which only use the lowest-frequency and highest-frequency invariant wavelet components instead of all.

Another method for estimating the fractal dimension using the wavelet transform is given by Espinal *et al.* [29]

$$D_j = \frac{\log\left(\sum_{u \in W_j} |u| \sqrt{2^{-j}}\right)}{j \log 2}, \qquad \text{with } j > 0. \tag{13}$$

Here D_j stands for the fractal dimension of wavelet component W_j and u for the pixel values that are element of W_j. The difference between the method of Alparone *et al.* and Espinal *et al.* is that the latter give an estimate of the fractal dimension of a part of the frequency spectrum, i.e., that part that is covered by wavelet component W_j. Alparone *et al.* estimate the fractal dimension of the whole spectrum; see also (10) and (11).

An advantage of the method of Espinal *et al.* is that it enables estimating multiple dimensions in the case of multifractal surfaces. On the other hand, this method is possibly correlated with the wavelet energy measures because there is a direct connection between the fractal dimension and wavelet energy.

4) Lacunarity: Another aspect of fractal surfaces is the lacunarity [15]; see also (9). Several methods exist to estimate the lacunarity [9], [17], [22], but a disadvantage of most methods is that they can only be applied to binary images (i.e., images with a depth of one bit). Therefore, images with a larger depth have to be thresholded first, introducing an extra parameter. Dobson *et al.* [9] extended the technique to scalar data and defined the lacunarity as

$$\Lambda(r) = \left(\frac{\sigma_x(r)}{\mu_x(r)}\right)^2 + 1. \tag{14}$$

Here σ_x and μ_x stand for the standard deviation and mean of the Σx of all windows (i.e., boxes) that cover the kernel from which the lacunarity is computed. r stands for the window size, from which Σx is determined. This indicates that the lacunarity is a function of the window size. If $r = 1$ (i.e., one pixel), the mean and standard deviation are equal to those obtained by (1), respectively (3).

5) Semivariogram: The semivariogram was chosen as an alternative for the well-known gray-level cooccurrence family of features because it gave better results on SAR data [4]. The semivariogram is defined by

$$\gamma(h) = \frac{1}{2N} \sum_{i=1}^{N} (x_i - x_{i+h})^2. \tag{15}$$

Here x_i stands for pixel i in the kernel that is examined, and x_{i+h} for the pixel at distance h from x_i. h is called the lag distance and can have any direction (e.g., east–west, north–south). The number N is the number of pixel pairs at distance h that can be found in the kernel.

B. Distributions and Variable Transformations

An important aspect of the discussed texture measures is their distribution or density function because that determines what sort of classifier must be used. Most classifiers are designed for normal distributions, but other classifiers can be designed. The situation becomes more complex when different measures, combined in one feature vector, have different types of distributions. Lining up these distributions is possible by applying variable transformations [14], but this can be difficult. The distribution of a texture measure is hard to foresee, and it is not always possible obtain the desired distribution. Another solution is to apply nonparametric techniques.

C. Nonparametric Classification

An example of a nonparametric classifier is the k nearest neighbor (kNN) classifier, which is based on the following distance [14]:

$$d_i^2 = (X - X_{i,\mathrm{NN}})^T \Sigma_i^{-1} (X - X_{i,\mathrm{NN}}). \tag{16}$$

Here $X_{i,\mathrm{NN}}$ is the kth nearest neighbor of class i to feature vector X under test and Σ_i the covariance matrix of class i. The smallest distance determines the class. This procedure is also referred to as the volumetric kNN procedure. For computational reasons, (16) can be simplified to

$$d_i^2 = \sum_{j=1}^{n} \frac{(x_j - x_{ij,\mathrm{NN}})^2}{\sigma_{ij}^2}. \tag{17}$$

Here x_j is the jth element of feature vector X with dimension n; $x_{ij,\mathrm{NN}}$ is the jth element of the kth nearest neighbor $X_{i,\mathrm{NN}}$; and σ_{ij} is the standard deviation of all jth elements of all sample feature vectors of class i.

D. Separability

To study the separability of features, in this paper the texture measures, a distance must be chosen that corresponds to the type of classifier that is used. For instance, for the Bayes quadratic classifier, the Bhattacharyya distance is most appropriate because both assume normal-distributed variables. In case of the kNN classifier in the previous section, a nonparametric separability measure is more appropriate. Fukunaga [14] gives different separability measures based on the within-class and between-class scatter matrices. Chosen is for the following distance:

$$J = \mathrm{tr}\left(S_w^{-1} S_{b,\mathrm{NN}}\right). \tag{18}$$

Here S_w is the within-class scatter matrix and $S_{b,\mathrm{NN}}$ the nonparametric between-class scatter matrix. tr stands for the trace. For the two-class case, the scatter matrices are defined as

$$\begin{aligned} S_w &= P_1 E[(X - M_1)(X - M_1)^T] \\ &\quad + P_2 E[(X - M_2)(X - M_2)^T] \\ &= P_1 \Sigma_1 + P_2 \Sigma_2 \end{aligned} \tag{19}$$

$$\begin{aligned} S_{b,\mathrm{NN}} &= P_1 E[(X_1 - X_{2,\mathrm{NN}})(X_1 - X_{2,\mathrm{NN}})^T] \\ &\quad + P_2 E[(X_2 - X_{1,\mathrm{NN}})(X_2 - X_{1,\mathrm{NN}})^T]. \end{aligned} \tag{20}$$

M_i stands for the mean of all sample feature vectors X of class i, Σ_i for the covariance matrix, and P_i for the *a priori* probability. $X_{i,\mathrm{NN}}$ is the kth nearest neighbor of class i but can be replaced by the mean of all k nearest neighbors if $k > 1$. If the *a priori* probabilities are equal, they are canceled in (18).

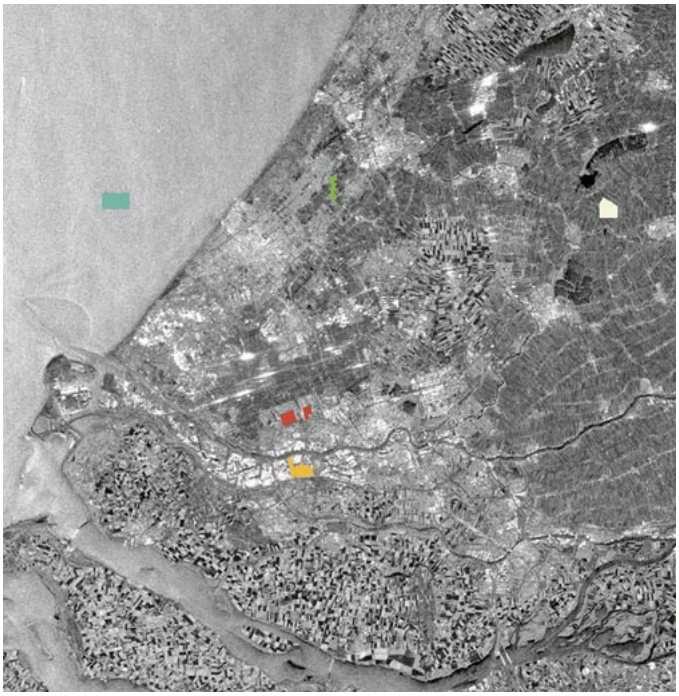

Fig. 1. ERS-1 SAR subimage of the Randstad Holland (UTM zone 31), including sample areas. Urban = red. Industry/greenhouses = orange. Forest = green. Water = blue. Other = light yellow.

TABLE I
NUMBER OF PIXELS PER CLASS SAMPLE AREA OF THE RANDSTAD HOLLAND

Class	NR. of Pixels
Other	7144
Urban	5837
Industry/greenhouses	6529
Forest	2656
Water	9472

E. Classifier Training

In classification, for map updating two training schemes can be used. One is to use the map itself to train the classifier [32]. Because the situation has changed so the satellite image does not correspond exactly with the map, always a certain degree of ambiguity between classes is introduced. Otherwise the map does not have to be updated. In case of parametric classification, this will not lead to serious errors if the parameters are not affected too much. With nonparametric classifiers as the kNN classifier, the situation is different. Every wrong chosen sample can influence the result dramatically, especially when k is small. A training scheme that is more appropriate here is to manually select a few unambiguous training areas [33].

III. Results and Discussion

A. SAR Image and Map

In order to analyze the results of the texture measures in Section II and to classify them for the purpose of map updating, an ERS-1 SAR image of the Randstad Holland and a corresponding

TABLE II
GENERALIZATION SCHEME OF VMAP1 OF THE RANDSTAD HOLLAND

Class	NR. of Pixels	Type Name [a]	Code [a]	Actual Type
Other	6050861	-	-	None, Pasture, Arable Land, Sand Dunes
		Foreshore	BA020	Beach
		Island	BA030	
Urban	1100865	Built-up Area	AL020	Residential, Commercial, Industrial
Green-houses	226346	Building	AL015	Greenhouses
Forest	192839	Orchard/Plantation	EA040	
		Trees	EC030	
Water	2932146	Lake/Pond	BH080	
		River/Stream	BH140	
		Water (Except Inland)	BA040	North Sea

[a]DIGEST-FACC.

Fig. 2. Generalized VMap1 of the Randstad Holland (UTM zone 31). Urban = red. Greenhouses = orange. Forest = green. Water = blue. Other = light yellow. Source: Topografische Dienst Nederland (TDN).

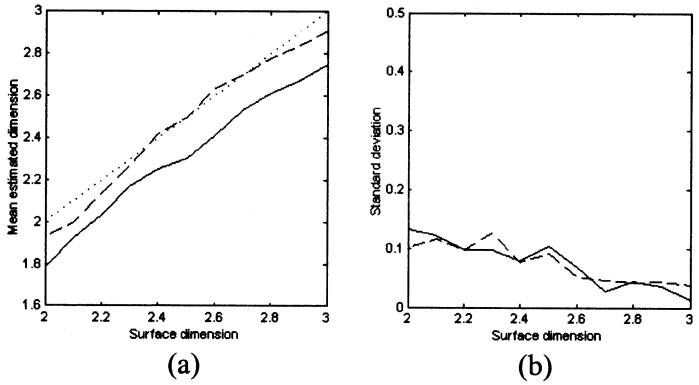

Fig. 3. Mean estimated fractal dimension (a) and standard deviation (b) using the method of linear regression (solid) and the one of Espinal *et al.* (dashed). The dotted line in (a) shows the ideal estimator.

digital map with scale 1 : 250 000 were used. ERS-1 operates in the C-band and is Vertical–Vertical (VV) polarized.

The ERS-1 SAR image of the Randstad Holland is the subset of a Precision Image (PRI) product [12]. The major characteristics of PRI images are ground-range, a pixel size of 12.5 m, and a resolution of 30 m. PRI images are processed as three nonoverlapping looks that are summed to reduce the speckle noise. The image was acquired June 23, 1995 (ERS-1 orbit 20601, frame 1035), and was logarithmically scaled. It was resampled to Universal Transverse Mercator (UTM) zone 31 using cubic convolution interpolation, 1 : 100 000 UTM paper maps of 1984, and a pixel spacing of 20 m. The size of the subimage is 3209×3273 pixels (64.2×65.5 km).

Based on existing land-cover and physical properties with respect to radar, five classes were defined: urban, industry/greenhouses, forest, water, and other. Industry and greenhouses both consist of large metal structures so they are physically similar. Fig. 1 shows the resampled ERS-1 SAR subimage, including the sample areas of the defined classes. Table I shows the number of pixels per sample area.

The image was not corrected for terrain elevation because the study area is rather flat (generally between -5 to 5 m with sand dunes up to 35 m along the coast). For ERS-1 this can result in a displacement of -12 to 82 m (up to four pixels).

The map of the Randstad Holland was obtained from VMap1 data, which was produced by the Topografische Dienst Nederland (TDN). VMap stands for Vector Map and 1 for the level that corresponds to a map scale of 1 : 250 000. VMap1 is specified by the National Imagery and Mapping Agency (NIMA) (http://www.nima.mil/) [18] and holds a subset of the Digital Geographic Information Exchange Standard—Feature and Attribute Coding Catalogue (DIGEST-FACC) [8]. Information on VMap is also given by Ohlhof *et al.* [20].

Ohlhof *et al.* did a more general study to the visibility of VMap1 entities in satellite imagery. Interpreting the results of this study, it appears that about one third of all VMap1 polygon entities could be identified by a human interpreter in ERS-1 imagery, which is not much. On the other hand, only two areas

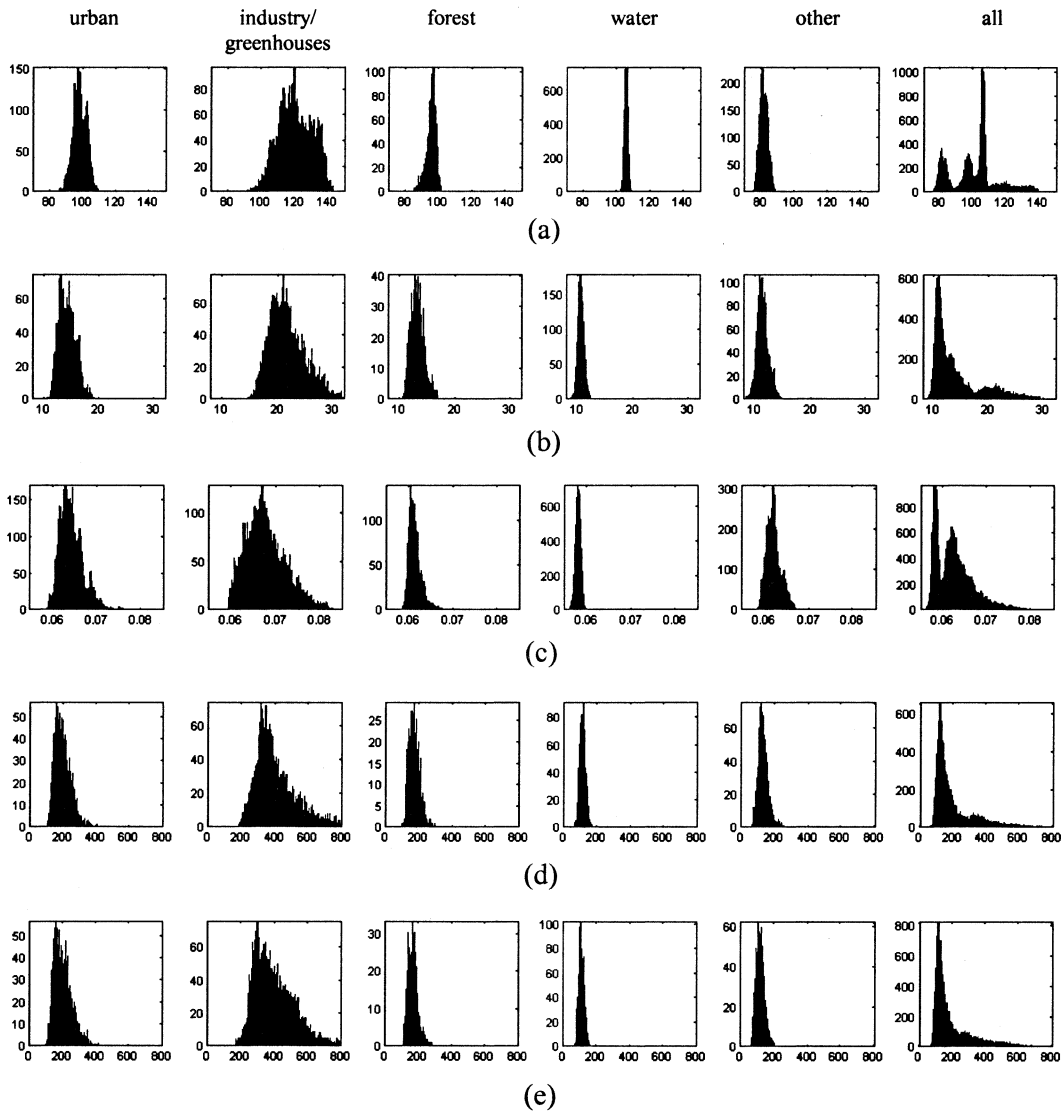

Fig. 4. Histograms of the sample areas of the ERS-1 SAR image in Fig. 1 of (a) the mean intensity, (b) variance, (c) weighted-rank fill ratio, (d) semivariogram east–west, lag distance 4, and (e) semivariogram north–south, lag distance 4.

were studied (Cologne, Germany and Minsk, Belarus) and the paper does not report on the level of experience of the human interpreter with ERS-1/2 data.

VMap1 data of The Netherlands [25] is extracted from the TOP250vector product of the TDN [3], [26]. Although the age of the TOP250vector data is not exactly known, it is not much older than 1998 because its review interval is four years [26]. Because some VMap1 land cover types are rather close, the map was conceptually generalized by merging areas with different codes into a map with less classes. Table II shows the merging rules and the number of pixels per class. For instance, forest includes the polygon types orchard/plantation and trees, which is conceptually valid for The Netherlands. An important difference with the classes defined in the ERS-1 image is that in the map industry falls in the class urban, while in the image it falls in the class industry/greenhouses. The map class other is wider than its ERS-1 sample area. The vector map was reprojected to UTM zone 31, and converted to a raster map with a grid cell size of 20 m. An image of the result is given by Fig. 2.

B. Texture Images and Separability

To create texture images, mean intensity, mean Euclidean distance, variance, skew, and kurtosis (1)–(5) were used from ERDAS Imagine [11]. The other measures [(6), (8), (10)–(15)] were implemented in ERDAS Imagine using the toolkit. Equation (7) was used for the wavelet energy measures.

Testing both fractal dimension estimators, the one using linear regression (10)–(12) and the one of Espinal *et al.* [29] (13), was done by generating ten series of 128×128 fractional Brownian surfaces according to the recipe of Keitt [30]. Each series consisted of eleven surfaces with a fractal dimension of 2.0 to 3.0 and a spacing of 0.1. The kernel size of both estimators was 16×16. Estimates were averaged to have one estimate per surface. For the estimator of Espinal *et al.* [29] was chosen for the highest wavelet component, which is the fourth level with this kernel $(j = 3)$. Fig. 3 shows the mean and standard deviation of the estimated dimensions. Fig. 3(a) shows that the linear regression estimate has a bias of about -0.2 compared to the ideal estimator. The highest level estimator of Espinal

TABLE III
$k = 1$ NONPARAMETRIC DISTANCE OF THE TEXTURE MEASURES BETWEEN THE LAND COVER CLASSES OF THE RANDSTAD HOLLAND IN THE ERS-1 IMAGE

texture measure	urban-other	ind/g-other	forest-other	water-other	ind/g-urban	forest-urban	water-urban	forest-ind/g	water-ind/g	water - forest	average
mean intensity	5.4678	11.1565	4.9043	94.1900	1.8727	0.0544	1.4581	4.1041	2.1073	6.4068	13.1722
mean Euclidean distance	0.0068	0.1115	0.0027	0.0001	0.0152	0.0007	0.0073	0.0358	0.1219	0.0031	0.0305
variance	0.1843	6.1040	0.0508	0.0691	1.4405	0.0084	2.1577	3.1976	10.9894	1.1297	2.5332
skew	0.1350	0.3672	0.0104	0.0004	0.0398	0.1748	0.2817	0.3761	0.4900	0.0013	0.1877
kurtosis	0.0027	0.0104	0.0006	0.0001	0.0017	0.0002	0.0005	0.0027	0.0045	0.0000	0.0023
entropy	0.0004	0.5431	0.0022	2.3854	0.4091	0.0002	3.3721	0.2944	3.6098	2.1255	1.2742
weighted-rank fill ratio	0.0728	0.5510	0.0000	2.4764	0.0137	0.0779	3.9032	0.5659	4.0900	2.0793	1.3830
wavelet energy level 0	6.0969	9.7841	6.0871	125.0935	1.9356	0.0961	1.5641	4.3052	2.3054	8.7677	16.6036
wavelet energy level 1	0.0034	0.3075	0.0002	0.0037	0.1485	0.0010	0.0487	0.2432	0.5846	0.0158	0.1357
wavelet energy level 2	0.0405	0.4909	0.0028	0.0001	0.0590	0.0022	0.0818	0.1656	0.6754	0.0098	0.1528
wavelet energy level 3	0.0443	0.8570	0.0013	0.0008	0.1679	0.0079	0.1282	0.5295	1.1920	0.0205	0.2949
fractal dimension (regr.)	0.0001	0.0029	0.0002	0.0104	0.0011	0.0002	0.0036	0.0030	0.0062	0.0078	0.0036
fractal dimension (Esp.)	0.0117	0.3258	0.0011	0.0008	0.0110	0.0018	0.0286	0.1154	0.4876	0.0095	0.0993
lacunarity index 2×2	0.0046	0.7761	0.0190	1.5093	0.4007	0.0001	2.3949	0.3392	2.8339	1.5231	0.9801
lacunarity index 3×3	0.0018	0.6916	0.0303	1.5163	0.4644	0.0033	2.0141	0.2816	2.2563	1.4591	0.8719
lacunarity index 4×4	0.0001	0.5809	0.0273	1.2118	0.4809	0.0114	1.4499	0.2086	1.9032	1.2537	0.7128
semivariogram e-w 1	0.1202	2.3586	0.0211	0.0006	0.2739	0.0795	0.3222	2.0602	3.2711	0.0599	0.8567
semivariogram e-w 2	0.1869	3.6915	0.1202	0.0293	0.3537	0.0811	1.0120	2.4882	6.3644	0.4463	1.4774
semivariogram e-w 4	0.0669	2.6319	0.0134	0.0555	0.6091	0.0093	1.1166	1.7375	5.0779	0.4531	1.1771
semivariogram e-w 8	0.0595	2.0380	0.0379	0.0652	0.7419	0.0008	0.8833	0.9854	3.4168	0.6029	0.8832
semivariogram e-w 12	0.0317	1.4949	0.0141	0.0361	0.5354	0.0002	0.4878	0.7132	2.6452	0.3540	0.6313
semivariogram n-s 1	0.3530	2.3252	0.0801	0.0003	0.4818	0.2518	0.5827	2.0756	2.5862	0.1064	0.8843
semivariogram n-s 2	0.5039	2.8437	0.0549	0.0016	0.4076	0.1972	0.8919	2.1802	3.2496	0.1751	1.0506
semivariogram n-s 4	0.4797	3.3544	0.1498	0.0058	0.5281	0.0281	1.1886	1.7493	4.2240	0.4782	1.2186
semivariogram n-s 8	0.1178	2.7785	0.0649	0.0554	0.9363	0.0010	1.2740	1.3144	4.2195	0.6519	1.1414
semivariogram n-s 12	0.1346	1.8439	0.0231	0.0000	0.4814	0.0087	0.1835	1.0272	1.9530	0.0382	0.5694

et al. [29] comes closer to the ideal estimator. Although the latter seems best in reproducing the fractal dimension, this does not necessarily mean that it gives the best separability as well.

After testing the other texture measures too, they were applied to the ERS-1 image of the Randstad Holland resulting in a series of texture images. The kernel size was 15×15 pixels (300×300 m) for all measures, except for the wavelet energy measures and the fractal dimensions. Here the kernel size was 16×16 pixels (320×320 m). Therefore, the wavelet energy could be determined of four levels ($j = 0$ to 3). The weighted-rank fill ratio was calculated for the 5% brightest pixels. The lacunarity for 2×2, 3×3, and 4×4 boxes. Semivariograms were determined in east–west and north–south directions for lag distances from 1 to 12. Because kernels of 15×15 and 16×16 pixels were used, the influence of the image speckle noise on the texture measures is minimal.

Fig. 4 shows the histograms of a selection of texture measures of the sample areas of the ERS-1 SAR image in Fig. 1. Most histograms illustrate that the distributions of the texture measures that are presented are not normal and not equal, which endorses the choice of the nonparametric techniques presented in Section II.

To study the separability of the texture measures between the classes of Table I, the nonparametric distance of (18) was used. Two cases have been worked out: $k = 1$ and $k = 11$. For $k = 11$, the mean of all 11 nearest neighbors was used (20). The results are given in Tables III and IV.

Interpreting Table III, far out the highest average score is achieved by the mean intensity (actually not a texture). Next are the variance, weighted-rank fill ratio, and semivariograms. The high average separability of the weighted-rank fill ratio is mainly caused by water. In case of water, entropy and lacunarity perform well too. Skew performs better than mean intensity in case of the combination urban–forest. The separabilities of the Euclidean distance, kurtosis, wavelet energy measures and fractal dimensions fall short. The separability of both fractal dimension estimators is quite different for some class combinations, but overall the estimator of Espinal *et al.* performs better. On the other hand, the level 3 wavelet component from which the latter is derived performs even better. The results of mean intensity and the wavelet energy of level 0 are quite similar, but that is because the level 0 wavelet component approximates the average value of the kernel. Urban, industry/greenhouses, and forest can best be distinguished from *other* by the mean intensity, variance, and the short-lag semivariograms. In case of water, mean intensity, entropy, weighted-rank fill ratio, and lacunarity perform well. Urban and industry/greenhouses can best be separated by mean intensity, variance, and longer lag semivariograms. Visually it is often hard to make a distinction between urban and forest from ERS-1/2 images. The measure that do best on these classes are skew, weighted-rank fill ratio, and the short-lag semivariograms. Forest and industry/greenhouses can best be separated by mean intensity, variance, and short-lag semivariograms. It is interesting to see that in most cases of the semivariograms, the lag direction does not really matter. The only exceptions are the cases with urban, which imply that the texture in its sample area is directional.

The results of the nonparametric separability in case of $k = 11$ in Table IV are quite similar to the case of $k = 1$ in Table III. Averaging the 11 nearest neighbors leads to a slightly improved separability. Comparison of Tables III and IV with the result of

TABLE IV
$k = 11$ NONPARAMETRIC DISTANCE OF THE TEXTURE MEASURES BETWEEN THE LAND COVER CLASSES OF THE RANDSTAD HOLLAND IN THE ERS-1 IMAGE

texture measure	urban-other	ind/g-other	forest-other	water-other	ind/g-urban	forest-urban	water-urban	forest-ind/g	water-ind/g	water - forest	average
mean intensity	6.0487	11.7810	5.5921	97.7877	1.9844	0.0702	1.5933	4.2543	2.1690	7.1646	13.8445
mean Euclidean distance	0.0148	0.1654	0.0062	0.0007	0.0312	0.0100	0.0194	0.1116	0.1984	0.0083	0.0566
variance	0.3149	6.8312	0.1059	0.0920	1.7054	0.0118	2.5072	3.4848	11.5759	1.4105	2.8040
skew	0.2158	0.4487	0.0186	0.0010	0.0542	0.3111	0.3124	0.4880	0.5128	0.0025	0.2365
kurtosis	0.0083	0.0207	0.0028	0.0008	0.0026	0.0008	0.0019	0.0052	0.0082	0.0003	0.0052
entropy	0.0025	0.6767	0.0070	2.6069	0.4490	0.0006	3.8416	0.3459	3.7213	2.3653	1.4017
weighted-rank fill ratio	0.0935	0.6217	0.0001	2.8137	0.0193	0.1018	4.1815	0.6441	4.2392	2.4172	1.5132
wavelet energy level 0	6.5810	10.0633	6.8224	128.3874	2.0973	0.1128	1.6785	4.4000	2.3448	9.5059	17.1993
wavelet energy level 1	0.0120	0.4072	0.0019	0.0082	0.1777	0.0044	0.0832	0.3235	0.6835	0.0354	0.1737
wavelet energy level 2	0.0796	0.6692	0.0098	0.0002	0.0814	0.0157	0.1029	0.3293	0.7540	0.0155	0.2058
wavelet energy level 3	0.0631	0.9569	0.0051	0.0020	0.2287	0.0211	0.1681	0.6909	1.3022	0.0422	0.3480
fractal dimension (regr.)	0.0009	0.0055	0.0021	0.0218	0.0024	0.0014	0.0079	0.0069	0.0136	0.0131	0.0076
fractal dimension (Esp.)	0.0192	0.4264	0.0045	0.0021	0.0209	0.0056	0.0504	0.2153	0.6707	0.0255	0.1441
lacunarity index 2×2	0.0065	0.8240	0.0254	1.6907	0.4440	0.0003	2.6480	0.3942	2.9097	1.6486	1.0591
lacunarity index 3×3	0.0026	0.7241	0.0366	1.5782	0.5075	0.0061	2.0784	0.3103	2.2755	1.4927	0.9012
lacunarity index 4×4	0.0004	0.6352	0.0387	1.2747	0.5522	0.0216	1.5135	0.2560	1.9229	1.2878	0.7503
semivariogram e-w 1	0.1632	2.6514	0.0497	0.0019	0.4441	0.0960	0.4359	2.2101	3.7030	0.1416	0.9897
semivariogram e-w 2	0.2232	4.0235	0.1860	0.0386	0.4835	0.1126	1.1498	2.8253	6.8160	0.6459	1.6504
semivariogram e-w 4	0.1061	2.9265	0.0319	0.0700	0.8176	0.0229	1.2449	2.0868	5.2591	0.5830	1.3149
semivariogram e-w 8	0.0791	2.1709	0.0542	0.0876	0.7868	0.0018	1.0491	1.0826	3.5689	0.7215	0.9603
semivariogram e-w 12	0.0458	1.6068	0.0214	0.0451	0.6483	0.0006	0.5550	0.8166	2.7341	0.4103	0.6884
semivariogram n-s 1	0.4089	2.4302	0.1236	0.0008	0.5724	0.2967	0.6687	2.1729	2.7004	0.1746	0.9549
semivariogram n-s 2	0.5495	2.9069	0.0797	0.0031	0.4837	0.2246	1.0034	2.2662	3.3503	0.2467	1.1114
semivariogram n-s 4	0.5403	3.4713	0.1871	0.0090	0.7024	0.0504	1.2980	1.9704	4.3523	0.5821	1.3163
semivariogram n-s 8	0.1398	2.8557	0.0953	0.0683	1.0387	0.0019	1.4202	1.3776	4.3322	0.8000	1.2130
semivariogram n-s 12	0.1727	1.9472	0.0359	0.0001	0.5552	0.0158	0.2114	1.1638	2.0158	0.0496	0.6168

TABLE V
NUMBER OF OBJECTS, USER ACCURACY PER CLASS, PERCENTAGE CORRECT CLASSIFIED (Pcc), AND KAPPA STATISTICS FOR FEW COMBINATIONS OF TEXTURE MEASURES OF THE CLASSIFICATION RESULT OF THE RANDSTAD HOLLAND. ALL STATISTICS ARE ON PER-PIXEL BASIS

texture measures	nr. of objects	user accuracy					Pcc	kappa
		urban	ind/g	forest	water	other		
mean	34521	20.7	4.5	3.3	82.8	88.3	43.8	25.3
mean+var	34281	31.1	10.2	4.1	96.8	86.8	51.7	36.1
mean+wfr	28910	35.3	11.3	4.3	94.9	87.5	51.2	36.0
mean+semivar	34251	28.3	9.3	4.1	95.7	86.9	50.6	35.2
mean+var+wfr	30628	28.9	10.7	5.2	96.4	87.6	52.4	37.1
mean+wfr+semivar	30625	24.1	9.6	5.3	95.7	87.8	51.5	35.9
mean+var+wfr+semivar	164925	24.1	10.2	6.0	96.7	87.4	52.1	36.3

[32] using the Bhattacharyya distance is meaningless. This can be done only for normal distributed texture measures.

C. Classification and Error Analysis

The best performing texture measures were selected for classification (i.e., mean intensity, variance, weighted-rank fill ratio, and semivariograms). In case of the semivariograms, east–west and north–south were used together for reasons of invariance, both with a lag distance of four. Chosen was an object-based approach using eCognition [31]. In this approach, objects are recognized first by applying region-growing segmentation. Input are the same texture images that are used for classification (e.g., if mean intensity and variance are used for classification, both are input for the segmentation process as well). Output are homogeneous objects with respect to the stack of input texture images. The number of output objects is dependent on the homogeneity. Table V shows the number of objects that were recognized from the $3209 \times 3273 = 10\,503\,057$ pixels. It shows that most input combinations lead to about 30 000 objects, except for the last combining all selected measures. The reason for that is that the last combination is less homogeneous than the others. Per object the average texture was computed.

Subsequently the objects were classified using (17). Chosen was for $k = 1$ because the difference in separability with $k = 11$ and the computation time are both minimal. Table V gives the user accuracy per class, the overall percentage correctly classified (Pcc) and the kappa statistics of a series of combinations, in comparison with the map of Fig. 2. Although the classification was object-based, all statistics were computed on a per-pixel basis. Fig. 5–8 show the results of some combinations. Not all objects were classified (maximum 0.2% of all pixels remained unclassified). For a few objects the minimum distance to at least two classes was equal, or the minimum distance was too large.

Table V shows that the classification results are not that accurate for all classes, although the overall accuracy improves

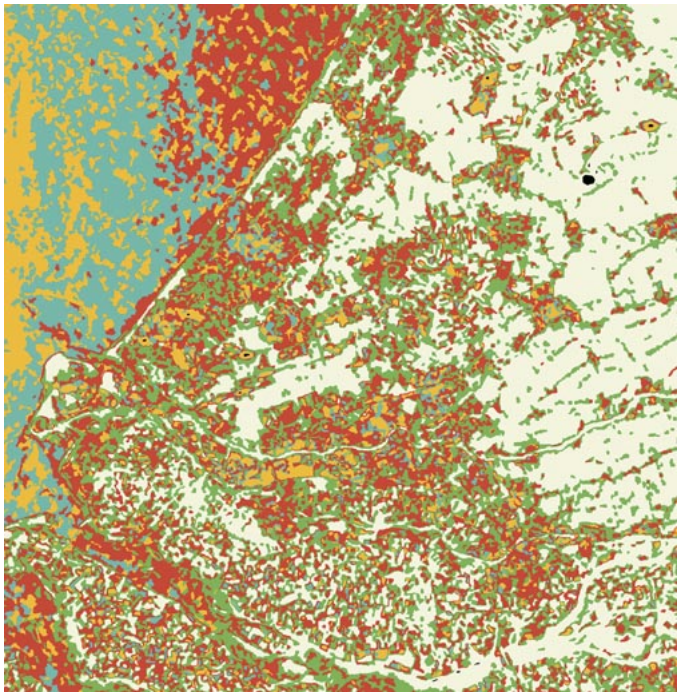

Fig. 5. Classification using mean intensity only.

Fig. 6. Classification using mean intensity and variance.

Fig. 7. Classification using mean intensity, variance, and weighted-rank fill ratio.

Fig. 8. Classification using mean intensity, variance, weighted-rank fill ratio, semivariogram east–west, and semivariogram north–south.

when adding any of the selected textures or combinations. Especially the scores of industry/greenhouses and forest are quite low, which means that the chance that a pixel is classified as industry/greenhouses or forest is actually industry/greenhouses or forest is low. But the scores of urban are low too (20% to 35%). This has several reasons. First there is a difference in definition of the classes in the map and the classification result. In case of the map, industry/greenhouses is covered by urban and greenhouses, which gives confusion. Second the map is not complete. If we look at the area between Rotterdam and the North Sea, the map shows *other*, while in reality it is full of harbor works and industrial activity (see also Fig. 1). In reality, there is more forest than on the map as well. Third is the low separability of urban–forest and urban–industry/greenhouses (see Table III/IV). The fact that urban, industry/greenhouses, and forest score low in accuracy can also be seen directly in Figs. 5–8.

The results of water are quite high but that is caused by the large area of water of the North Sea. Inland water is seldom classified as water. The reason for that is that the backscatter of the sea surface is different from that of inland water due to the wind state. The class other is classified with an accuracy of 86% to 88%, but when looking at Figs. 5–8, it is often classified as urban or forest in case of arable land (see also Fig. 1). The reason for that is that arable land gives much texture in June due to differences in crops, growth and density.

IV. Conclusion

In this paper, an overview of modern texture measures is given and applied to ERS-1 satellite SAR data of the Randstad Holland in The Netherlands for the purpose of map updating. The Randstad Holland can be characterized as a well-planned dispersed urban area. In a separability analysis of a set of defined land-cover classes, the measures that performed best were mean intensity (actually no texture), variance, weighted-rank fill ratio, and semivariograms. Because most texture distributions were not normal, those chosen were for nonparametric techniques: a k nearest neighbor classifier with corresponding separability measure. The accuracy of classification was determined using the map.

Results showed that the best performing textures improve classification. However, the maximum overall percentage of correct classification was not optimal. Three reasons for that were found. First, the defined classes were not exactly the same as defined in the map. So did industry fall in the class industry/greenhouses in the image and in urban with the map. Second, the map showed deficiencies. Some large harbor works and industrial areas were not included. Third is the low separability of some classes, especially of urban and forest, and of urban and industry/greenhouses, which indicates that the land-cover information content of ERS-1 leaves something to be desired.

An interesting question is if future high-resolution radar satellites as the ones mentioned in the Introduction provide more land-cover texture to improve the classification accuracy. Unfortunately, this question cannot be answered yet, unless data from airborne radar sensors are used.

References

[1] L. Alparone, M. Barni, M. Betti, and A. Garzelli, "Fuzzy clustering of textured SAR images based on a fractal dimension feature," in *Proc. IGARSS*, 1997, pp. 1184–1186.

[2] M. Bellagente, P. Gamba, and P. Savazzi, "Fuzzy texture characterization of urban environments by SAR data," in *Proc. IGARSS*, 1999, pp. 1232–1234.

[3] B. Bruns, *Extraction Guide Top250 Vector—VmapLevel1, Version 1.2*: Topografische Dienst Nederland (TDN), Dec. 1997.

[4] J. R. Carr and F. P. de Miranda, "The semivariogram in comparison to the co-occurrence matrix for classification of image texture," *IEEE Trans. Geosci. Remote Sensing*, vol. 36, pp. 1945–1952, Nov. 1998.

[5] C. K. Chui, Ed., *Wavelets: A Tutorial in Theory and Applications*. San Diego, CA: Academic, 1992.

[6] S. R. Cloude and E. Pottier, "A review of target decomposition theorems in radar polarimetry," *IEEE Trans. Geosci. Remote Sensing*, vol. 34, pp. 498–518, Mar. 1996.

[7] R. J. Dekker, "Monitoring the urbanization of Dar Es Salaam using ERS SAR data," in *Int. Arch. Photogramm. Remote Sens.*, 2000, vol. 32, pp. 62–69.

[8] Digital Geographic Information Exchange Standard (DIGEST), ed. 2.1 (2000, Sept.). [Online]. Available: http://www.digest.org/

[9] C. Dobson, L. Pierce, J. Kellndorfer, and F. Ulaby, "Use of SAR image texture in terrain classification," in *Proc. IGARSS*, 1997, pp. 1180–1183.

[10] Y. Dong, B. C. Forster, and C. Ticehurst, "A new decomposition of radar polarization signatures," *IEEE Trans. Geosci. Remote Sensing*, vol. 36, pp. 933–939, May 1998.

[11] ERDAS, *ERDAS Field Guide*, 5th ed. Atlanta, GA: ERDAS Inc., 1999.

[12] ESA, "ESA ERS-1 Product Specification," ESA, Noordwijk, The Netherlands, SP-1149, Issue 3.0, June 1992.

[13] A. Freeman and S. L. Durden, "A three-component scattering model for polarimetric SAR data," *IEEE Trans. Geosci. Remote Sensing*, vol. 36, pp. 963–973, May 1998.

[14] K. Fukunaga, *Introduction to Statistical Pattern Recognition*, 2nd ed. San Diego, CA: Academic, 1990.

[15] H. J. H. Kux and G. M. Henebry, "Multi-scale texture in SAR imagery: Landscape dynamics of the pantanal, Brazil," in *Proc. IGARSS*, 1994, pp. 1069–1071.

[16] A. Laine and J. Fan, "Texture classification by wavelet packet signatures," *IEEE Trans. Pattern Anal. Machine Intell.*, vol. 15, pp. 1186–1191, Nov. 1993.

[17] B. Lin and Z. R. Yang, "A suggested lacunarity expression of Sierpinski carpets," *J. Phys. A: Math. Gen.*, vol. 19, pp. L49–L52, 1986.

[18] NIMA, "Vector map (VMAP) level 1," National Imagery and Mapping Agency (NIMA), Rep. MIL-PRF-89 033, June 1995.

[19] L. M. Novak, G. J. Owirka, and C. M. Netishen, "Performance of a high-resolution polarimetric SAR automatic target recognition system," *Lincoln Lab. J.*, vol. 6, no. 1, pp. 11–23, 1993.

[20] T. Ohlhof, T. Emge, W. Reinhardt, K. Leukert, C. Heipke, and K. Pakzad, "Generation and update of VMAP data using satellite and airborne imagery," in *Int. Arch. Photogramm. Remote Sens.*, 2000, vol. 32, pp. 762–768.

[21] A. P. Pentland, "Fractal-based description of natural scenes," *IEEE Trans. Pattern Anal. Mach. Intell.*, vol. 6, pp. 661–674, June 1984.

[22] R. E. Plotnick, R. H. Gardner, and R. V. O'Neill, "Lacunarity indices as measures of landscape texture," *Landscape Ecol.*, vol. 8, pp. 201–211, 1993.

[23] M. Santoro, A. Fanelli, J. Askne, and P. Murino, "Monitoring urban areas by means of coherence levels," in *Proc. FRINGE'99— Advancing ERS SAR Interferometry from Applications Toward Operations, Centre Spatial de Liege*, Liege, Belgium, Nov. 1999.

[24] C. V. Stewart, B. Moghaddam, K. J. Hintz, and L. M. Novak, "Fractal Brownian motion models for synthetic aperture radar imagery scene segmentation," *Proc. IEEE*, vol. 81, pp. 1511–1522, Oct. 1993.

[25] TDN, "Vector Smart Map (VMAP1)," Topografische Dienst Nederland (TDN), CD 049-NL, 1st ed., 1998.

[26] Digital Products (Vector Files), TDN. [Online]. Available: http://www.tdn.nl/

[27] H. Unser, "Sum and difference histograms for texture classification," *IEEE Trans. Pattern Anal. Machine Intell.*, vol. 8, pp. 118–125, Jan. 1986.

[28] C. E. Woodcock and A. H. Strahler, "The factor of scale in remote sensing," *Remote Sens. Environ.*, vol. 21, pp. 311–322, 1987.

[29] F. Espinal, B. D. Jawerth, and T. Kubota, "Wavelet-based fractal signature analysis for automatic target recognition," *Opt. Eng.*, vol. 37, no. 1, pp. 166–174, 1998.

[30] T. H. Keitt, "Spectral representation of neutral landscapes," *Landscape Ecol.*, vol. 15, pp. 479–493, 2000.

[31] Definiens Imaging GmbH, *eCognition 2.1 User Guide*. München, Germany: Definiens Imaging GmbH, 2002.

[32] R. J. Dekker, "Texture analysis of urban areas in ERS SAR imagery for map updating," in *Proc. IEEE/ISPRS Joint Workshop on Remote Sensing and Data Fusion Over Urban Areas (URBAN 2001)*, Rome, Italy, Nov. 8–9, 2001, pp. 226–230.

[33] ——, "Texture analysis and classification of SAR images of urban areas," in *Proc. IEEE/ISPRS Joint Workshop on Remote Sensing and Data Fusion Over Urban Areas (URBAN 2003)*, Berlin, Germany, May 22–23, 2003, pp. 258–262.

Rob J. Dekker received the B.S. degree in electrical engineering from the Hogeschool Rotterdam, The Netherlands, and the M.S. degree in geographical information systems from the Vrije Universiteit Amsterdam, The Netherlands, in 1990 and 2003, respectively.

Since 1991, he has been with the TNO Physics and Electronics Laboratory, The Hague, The Netherlands, where he has worked on synthetic aperture radar signal and image processing, polarimetric calibration, various remote sensing projects, change detection, and automatic target detection and recognition. His current interests include remote sensing image analysis, urban monitoring, and geographical information systems.